HiSST: International Conference on
High-Speed Vehicle Science Technology
26–29 November 2018, Moscow, Russia

# Numerical Simulation of Mass Addition Effect on Heat Transfer of Descent Space Vehicle

*Ivan V. Egorov*[1,2], *Natalia V. Palchekovskaya*[1,2]

## Abstract

Numerical study of mass addition influence on heat transfer of two models of descent space vehicle at hypersonic flow regimes is carried out. Numerical simulation is fulfilled using Navier-Stokes equations in axisymmetric statement. The first model geometry and flow conditions are correspond to those in experimental work [1], and the second model corresponds to descent space vehicle of ExoMars project. Various mass flow rates are considered in order to investigate effect of gas injection on values of heat flux. Calculations are carried out using in-house software package HSFlow. Comparison of the results with experimental results [1] and numerical results of other authors is made.

**Keywords**: numerical simulation, mass addition, heat transfer, space vehicle, hypersonic flow

## Nomenclature

***B*** **–** Source vector
***E*** **–** Flux vector in x direction
***G*** **-** Flux vector in y direction
$H$ – Total enthalpy
$J$ - Transformation Jacobian
**I** – Heat flux vector
$L$ – Characteristic linear size
$M$ – Gas molar weight
M – Mach number
$R$ – Universal gas constant
Re – Reynolds number
***Q*** **–** Vector of conservative dependent values
$T$ – Temperature
**V** **–** Velocity vector
$c_p$ – specific heat capacity at constant pressure
$e$ – Total energy per unit volume
$h$ - Static enthalpy
m – mass addition
$p$ – Pressure
$r$ - distance
***s*** – Strain velocity tensor
$t$ - Time
$u$ – Velocity component in x direction
$v$ – Velocity component in y direction
$\xi$ - Longitudinal curvilinear coordinate
$\eta$ - Normal curvilinear coordinate
$\lambda$ - Coefficient of thermal conductivity
$\mu$ - Coefficient of molecular viscosity
$\rho$ - Density
$\tau$ - Symmetric tensor of viscous stresses
c – Cartesian
w –Wall
$\infty$ - Free stream value
* - nominal value

## 1. Introduction

During descent of a space vehicle at hypersonic regimes high levels of heat flux arise, leading to strong heating of the vehicle surface. It is well known that ablative heat-shielding is used for heat removal in order to reduce surface heating. Also, heat-shielding systems, producing mass addition into boundary layer, are applied. Heat-shielding systems effectively decrease temperature of the

[1] *Central Aerohydrodynamic Institute, 1 Zhukovsky street, Zhukovsky, Moscow region, Russia,* natalia.palchekovskaya@tsagi.ru
[2] *Moscow Institute of Physics and Technology, 9 Institutsky pereulok, Dolgoprudny, Moscow region, Russia,* palchekovskaia.nv@mipt.ru

space vehicle on the flow regimes with high-level heating. However, mass addition also may result in early laminar-turbulent transition, and, as consequence, sharp increase of aerodynamic heating. In this work two space vehicle models are considered: the simplified hemispherical model [1] of space vehicle and real model of descent space vehicle for Mars exploration.

## 2. Governing equations

Numerical simulation of the problem is based on the solution of axisymmetrical Navier-Stokes equations. In arbitrary curvilinear coordinate system ($\xi$, $\eta$), where $x = x(\xi, \eta)$, $y = y(\xi, \eta)$ - Cartesian coordinates, axisymmetrical Navier-Stokes equations are written in divergent form as:

$$\frac{\partial \boldsymbol{Q}}{\partial t} + \frac{\partial \boldsymbol{E}}{\partial \xi} + \frac{\partial \boldsymbol{G}}{\partial \eta} = \boldsymbol{B} \qquad (1)$$

Vectors $\boldsymbol{E}$, $\boldsymbol{G}$ are related to corresponding vectors $\boldsymbol{E}_c$, $\boldsymbol{G}_c$ in Cartesian coordinate system by formulas:

$$\boldsymbol{Q} = J\boldsymbol{Q}_c,\ \boldsymbol{E} = J\left(\boldsymbol{E}_c \frac{\partial \xi}{\partial x} + \boldsymbol{G}_c \frac{\partial \xi}{\partial y}\right),\ \boldsymbol{G} = J\left(\boldsymbol{E}_c \frac{\partial \eta}{\partial x} + \boldsymbol{G}_c \frac{\partial \eta}{\partial y}\right)$$

where $J = \partial(x, y) / \partial(\xi, \eta)$ – transformation Jacobian.

Cartesian components of vectors $\boldsymbol{E}_c$ and $\boldsymbol{G}_c$ for axisymmetrical Navier-Stokes equations are as follows:

$$\boldsymbol{Q}_c = \begin{pmatrix} \rho \\ \rho u \\ \rho v \\ \rho e \end{pmatrix},\ \boldsymbol{E}_c = \begin{pmatrix} \rho u \\ \rho u^2 + p + \tau_{xx} \\ \rho uv + \tau_{xy} \\ \rho uH + I_x \end{pmatrix},\ \boldsymbol{G}_c = \begin{pmatrix} \rho v \\ \rho uv + \tau_{xy} \\ \rho v^2 + p + \tau_{yy} \\ \rho vH + I_y \end{pmatrix}$$

where $e = h - p/\rho + (u^2 + v^2)/2$ – total energy per unit volume; $H = h + (u^2 + v^2)/2$ – total enthalpy, $h = c_p T$ – static enthalpy; $\boldsymbol{\tau}$ – symmetric tensor of viscous stresses, related to strain velocity tensor $\mathbf{s}$ by linear dependency

$$\boldsymbol{\tau} = -\mu \mathbf{s}$$

Heat flux vector $\mathbf{I}$ is defined by expression

$$\mathbf{I} = -\lambda \mathrm{grad}(T) + \boldsymbol{\tau}\mathbf{V}$$

System of equations (1) is closed by the equation of state and by dependencies of transport coefficients on temperature and pressure. In this work perfect gas model is used.
Initial-boundary problem, formulated above, is solved numerically on basis of finite-volume method. For monotone difference scheme flux calculation in half-integer nodes is carried out on basis of Riemann problem solution. This problem comes to solution of nonlinear set of algebraic equations. For approximation of convective component of flux vectors in half-integer nodes monotone Godunov scheme and approximate Roe technique for Riemann problem solution are used. To increase

approximation order for interpolation of dependent variables on edge of elementary cell minimum derivatives principle (MUSCL) is used. For approximation of diffusive component of flux vectors **E** and **G** on the edge of elementary cell central difference scheme of second order accuracy is applied. Calculations are fulfilled for perfect gas model using in-house software package HSFlow [2 - 4].

## 3. Results of numerical simulation

### 3.1. Simulation of flow over hemispherical model

In this work hypersonic flow over space vehicle model, having hemispherical shape (R = 0.0089 m ) with cylindrical extension (Fig. 1), is considered. Ablation is simulated by normal gas injection into the boundary layer. Main flow parameters, considered in this work, correspond to experimental work [1] and presented in Table 1. On the body surface isothermal boundary conditions with $T_w$ = 300 K and non-slippery boundary conditions are set. Mass addition along the surface is given by dependency, obtained by interpolation of experimental values [1] (Fig.2). On the outer boundary Dirichlet boundary conditions are set, on the axis of symmetry – symmetrical boundary conditions, on the outflow boundary - non-reflecting boundary conditions.

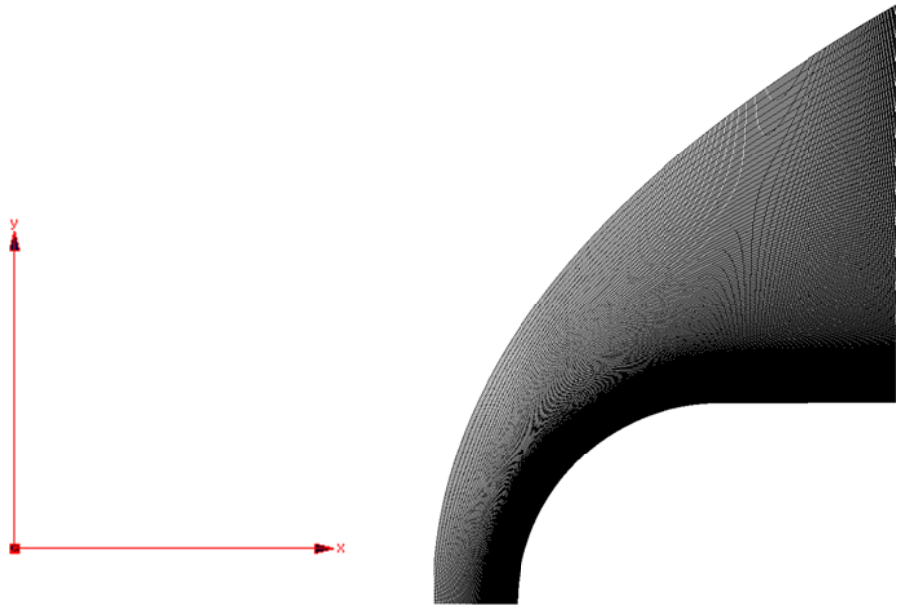


**Fig 1.** Geometry and computational grid for the hemispherical model

Table 1

| Regime No. | $Re_1$ ($m^{-1}$) | $M_\infty$ | $m^*$ | $T_\infty$ (K) |
|---|---|---|---|---|
| 1 | $6.24\times10^6$ | 7.32 | 0.00 | 66.74 |
| 2 | $6.24\times10^6$ | 7.32 | 0.003 | 66.74 |
| 3 | $6.24\times10^6$ | 7.32 | 0.007 | 66.74 |
| 4 | $1.288\times10^7$ | 7.32 | 0.00 | 66.74 |
| 5 | $1.288\times10^7$ | 7.32 | 0.004 | 64.95 |
| 6 | $1.331\times10^7$ | 7.32 | 0.01 | 63.84 |
| 7 | $1.191\times10^7$ | 7.32 | 0.013 | 68.00 |

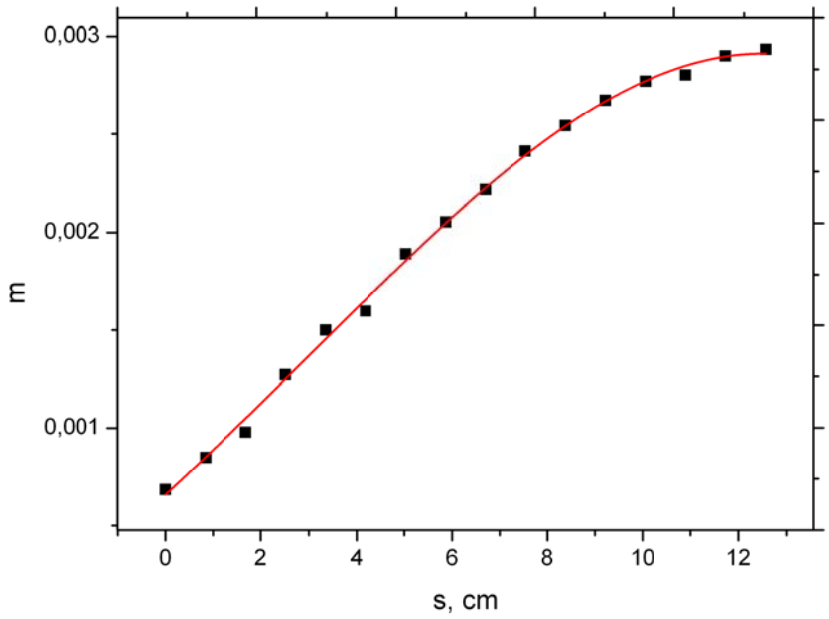


**Fig 2.** Distribution of the mass flow rate at the nominal value of mass addition $m^* = 0.003$. The black squares – experiment [1], red curve – approximation for calculations

When injection takes place, it is seen from temperature field that normal injection leads to cold gas displacement from the vehicle surface. Gas injection also leads to small shift of the shock wave position (Fig. 3).

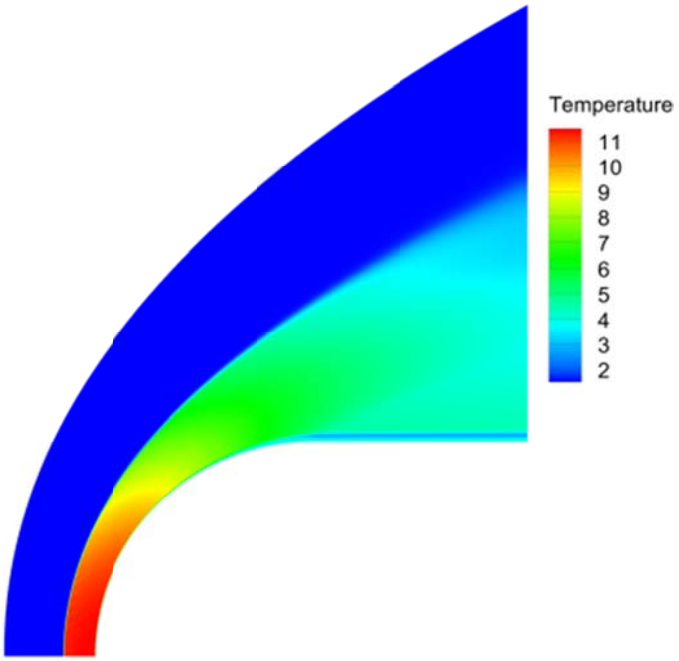


**Fig 3.** Temperature field at the nominal value of mass addition $m^* = 0.013$

The main purpose of the current work is study of normal injection influence on heat transfer in the vicinity of the space vehicle model. In Fig.4 distributions of normalized heat flux along the surface at values of nominal mass addition $m^*$ from 0 to 0.007 and unit Reynolds number $Re_{1\infty} = 6.24\times10^6$ $m^{-1}$ are given. Solid lines correspond to computational results, obtained using in-house software package HSFlow, symbols designates experimental data (see [1]). Heat flux values are normalized using the value of heat flux at the stagnation point for the case without gas injection. It can be seen that for flow regimes without gas injection ($m^* = 0$) and with small value of gas injection ($m^* = 0.003$) numerical values of heat flux are in good agreement with experimental data. With increase of nominal value of mass addition ($m^* = 0.007$) numerical values of heat flux substantially differ from experimental ones in the vicinity of the stagnation point. The reason of such discrepancy may consist in a poor accuracy of mass addition measurement in the vicinity of the stagnation point in the experiment [1].

Distributions of normalized heat flux for regimes with nominal mass addition values $m^*$ from 0 to 0.013 and unit Reynolds number $Re_{1\infty} = 1.331\times10^7$ $m^{-1}$ are presented in Fig.5. Here results, obtained using in-house code HSFlow, are compared with numerical results of work [5] and experimental results of work [1]. Heat flux distributions, obtained from HSFlow solutions and solutions of work [5], have good agreement in peak values of heat flux at stagnation point (discrepancy no more than 10%). But they have appreciable difference on the most length of hemispherical header. The reason of this discrepancy cannot be clearly understood, because of lack of information about numerical methods and computational grids used in work [5]. From Fig. 7 it can be seen that for low values of mass addition ($m^* = 0$ and $m^* = 0.004$) numerical results are in good agreement with experimental data. With increase of mass addition values ($m^* = 0.01$ and $m^* = 0.013$) numerical results have no agreement with experiment in the vicinity of stagnation point, but at $s > 0.4$ satisfactory agreement of numerical and experimental results is observed. It should be noted that in experiment mass addition values $m^* = 0.01$ and $m^* = 0.013$ corresponds to regimes with laminar-turbulent transition, which initiates at $s \approx 0.9$ and $s \approx 0.7$ correspondingly. Explanation of the appreciable difference in numerical and experimental heat fluxes in stagnation point region may consist in fact that real mass addition values in experiment are less than mentioned in the work [1].

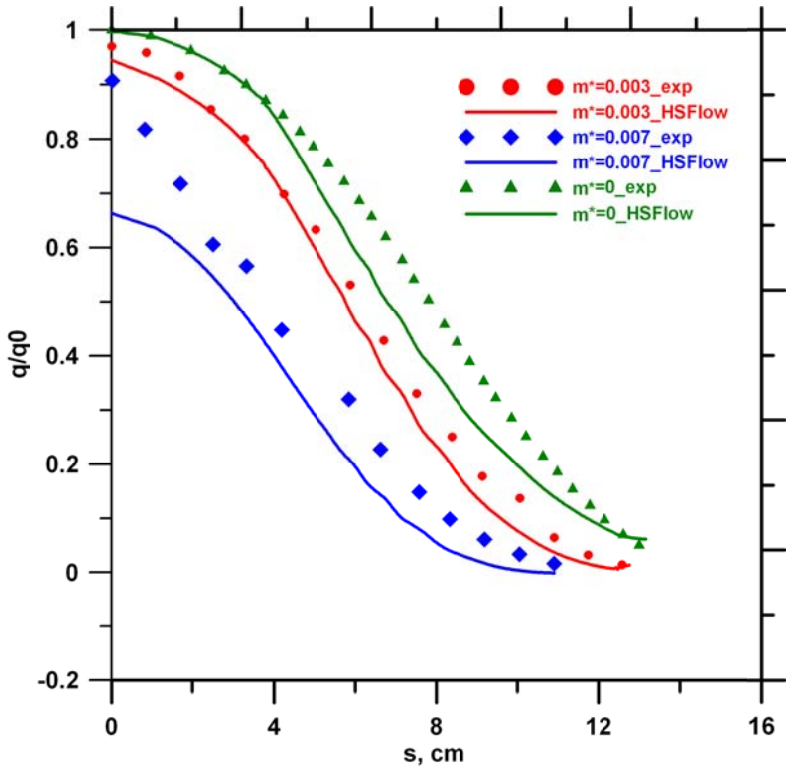

**Fig 4.** Experimental an numerical normalized heat flux distributions for nominal mass addition values $m^*$ = 0, 0.003 and 0.007

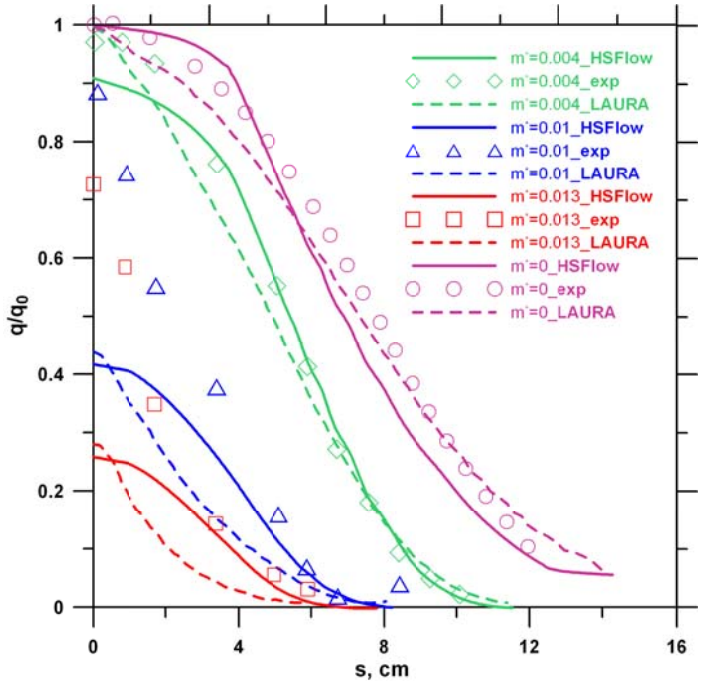


**Fig 5.** Experimental and numerical distributions of the normalized heat flux for nominal mass addition values $m^*$ = 0, 0.004, 0.01 and 0.013

In Fig.6 profiles of full velocity near the point of spherical and cylindrical parts conjunction are shown. These profiles demonstrate evolution of velocity behavior with increase of mass addition value. For the case without injection ($m^*$ = 0) full velocity profile has no inflection points and, thus boundary layer doesn't support any significant enhancement of instability modes. For $m^*$ = 0.004 inflection point can hardly been detected, but at $m^*$ = 0.013 inflection in the velocity profile is well seen. This fact may indicate the presence of instability modes in boundary layer.

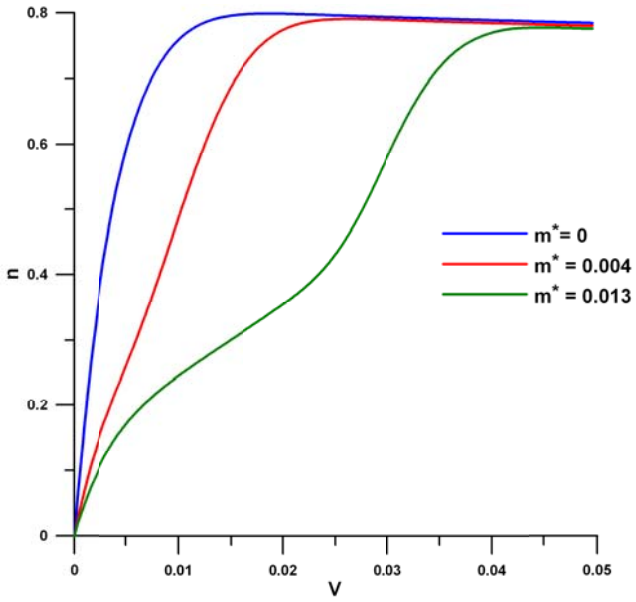

**Fig 6**. Full velocity profiles for three mass addition values: 0, 0.004, 0.013

### 3.2. Simulation of flow over Martian descent space vehicle

Using results, obtained for hemispherical model, simulation flow over descent space module of ExoMars (Fig. 7) project with mass addition is carried out. Flow regimes are chosen with free stream Mach number range $M_\infty = 7 \div 10$, unit Reynolds number range $Re_1 \approx 10^6 \div 10^7$ $m^{-1}$ and mass flow rates range $m^* = 0 \div 0.1$. In Fig. 8 distribution of normalized heat flux along the model of Marsian space vehicle is given. These dependencies show effect of gas injection and suction on value of heat flux. It is seen that with increase of injection values from $m = 10^{-3}$ to $m = 10^{-2}$ decrease of heat flux values is observed; with increase of absolute suction values heat flux increases.

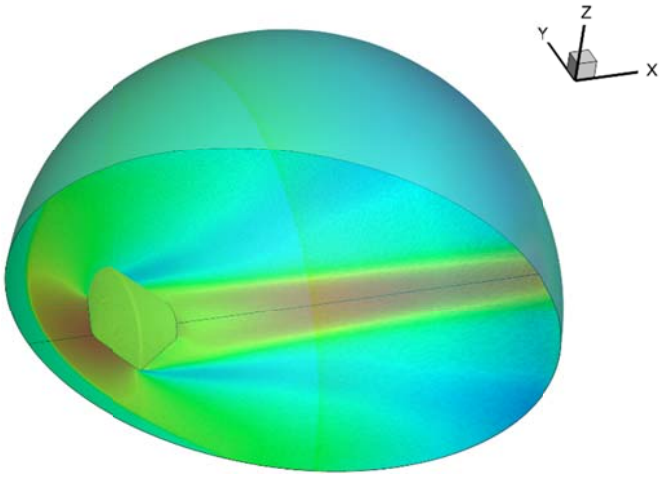


**Fig 7.** Model of the space vehicle ExoMars and computational domain

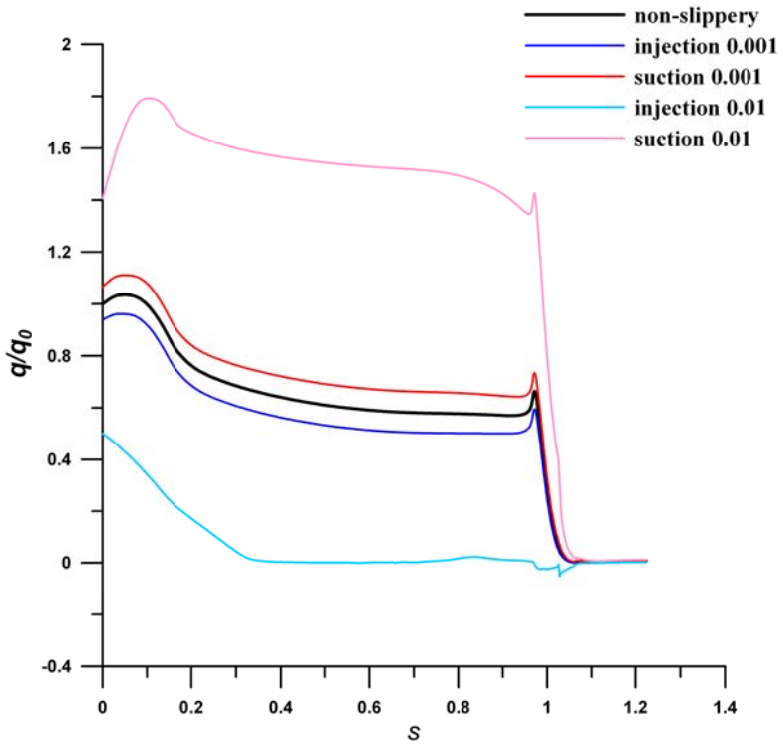

**Fig 8.** Computational normalized heat flux distributions: black – non-slippery, blue – m = $10^{-3}$, light blue – m = $10^{-2}$, red – m = $-10^{-3}$, pink – m = $-10^{-2}$

## 4. Conclusions

In this work numerical solution of axisymmetrical Navier-Stokes equations with mass addition to the boundary layer is carried out in order to study effect of ablation on heat transfer on the models of descent space vehicles. Peculiarities of flow fields for wide range of mass flow rates are studied. Comparison of heat flux distributions, obtained in this study, with experiment [1] and numerical investigations [5] is fulfilled. It is shown that at low values of mass addition experimental and numerical heat fluxes are in good agreement. But for higher values of mass addition numerical heat flux decreases much stronger than experimental one. This result can be explained by the fact that real mass addition values in experiment are less than indicated in the work [1].

The reported study was funded by RFBR according to the research project № 17-08-00969 (the problem statement and calculations) and was supported by the Russian Science Foundation project no. 17-79-10438 (computational technique development).

## References

1. Kaattari, G.E.: Effects of mass addition on blunt-body boundary-layer transition and heat transfer. NASA Technical Paper 1139 (1978)
2. Bashkin, V.A., Egorov, I.V.: Numerical simulation of the viscous perfect gas dynamics. Fizmatlit, Moscow (2012)
3. Egorov, I.V., Novikov, A.V., Palchekovskaya, N.V.: Numerical simulation of the flow over a segment-conical body on the basis of Reynolds equations. Computational Mathematics and Mathematical Physics. 58, 118-129 (2018)
4. Bashkin, V.A., Egorov, I.V., Palchekovskaya, N.V.: The interaction of shock waves with a boundary layer on a sharp plate and a blunted plate. High Temperature. 54, 356- 369 (2016)
5. Thompson, R.A., Gnoffo, P.A.: Implementation of a Blowing Boundary Condition in the LAURA Code. Proc. of 46th AIAA Aerospace Sciences Meeting and Exibit. AIAA 2008 – 1243, 1-11 (2008)